https://doi.org/10.1016/j.ymssp.2020.106831

A novel damage characterization approach for laminated composites in the absence of material and structural information

Maosen Cao[1,2], Zhongqing Su[3], Hao Xu[4],

Maciej Radzieński[5], Wei Xu[1,3,2*], Wiesław Ostachowicz[5]

[1] Jiangxi Provincial Key Laboratory of Environmental Geotechnical Engineering and Disaster Control, Jiangxi University of Science and Technology, Ganzhou 341000, People's Republic of China

[2] Department of Engineering Mechanics, Hohai University, Nanjing 210098, People's Republic of China

[3] Department of Mechanical Engineering, The Hong Kong Polytechnic University, Hung Hom, Kowloon, Hong Kong, People's Republic of China

[4] School of Aeronautics and Astronautics, Faculty of Vehicle Engineering and Mechanics, State Key Laboratory of Structural Analysis for Industrial Equipment, Dalian University of Technology, Dalian 116024, People's Republic of China

[5] Institute of Fluid-Flow Machinery, Polish Academy of Sciences, Gdańsk 80-231, Poland

*Corresponding author.

E-mail addresses: cmszhy@hhu.edu.cn (M. Cao); zhongqing.su@polyu.edu.hk (Z. Su); xuhao@dlut.edu.cn (H. Xu); maciej.radzienski@imp.gda.pl (M. Radzieński); weixu@polyu.edu.hk, wxu@hhu.edu.cn (W. Xu); wieslaw.ostachowicz@imp.gda.pl (W. Ostachowicz)

Abstract: Laminated composites have been increasingly used in structural components. However, transverse impact to a composite laminate can cause initial damage such as notches and delamination, jeopardizing the integrity and safety of composite laminated structures. With this concern, this study proposes a novel damage characterization approach for the identification of initial damage in composite laminates, even in the absence of material and structural information. In particular, starting from the vibration equation of composite laminates, a novel concept of damage-caused force is formulated to characterize damage, and strategies of isotropization and normalization are further integrated to deal with the absence of material and structural information, respectively. Thereby, a baseline-free damage index is established using the damage-caused force, by which the presence, location, and size of initial damage in cross-ply composite laminates can be characterized without knowledge of material and structural parameters. The capability of the approach is numerically verified on carbon fiber-reinforced polymer (CFRP) laminates with a notch and a delamination, respectively. The applicability of the approach is experimentally validated by identifying a notch and a delamination in CFRP laminates, respectively. The CFRP laminates are excited by lead-zirconate-titanate (PZT) actuators and scanned by a scanning laser vibrometer (SLV) to acquire high-resolution mode shapes. Numerical and experimental results show that the proposed approach features high robustness to environmental noise and is capable of identifying initial damage in cross-ply composite laminates without prior material and structural information.

***Keywords*:** composite laminate; initial damage identification; mode shape; damage-caused force; damage index; laser scanning measurement

1 Introduction

Laminated composites have been increasingly used in large-scale structural components, such as wind turbine blades, due to their high strength and low density. However, initial damage such as notches and delamination can be caused when composite laminates are subjected to transverse impact. With this concern, there is a great need to identify such damage in the early stage to prevent initial damage from developing to a significant degree, jeopardizing the integrity and safety of composite laminated structures [1, 2].

In past decades, nondestructive testing techniques such as X-ray [3], C-scan [4], ultrasonic imaging [5], strain [6-10], eddy current [11, 12], electrical potential [13], thermography [14-17], shearography [18], guided wave [19-23], and vibro-acoustics [24-28] approaches have been widely developed for damage detection in laminated composites. However, their common limitation is that the approximate damage region needs to be known *a priori* [29]. In recent years, damage identification methods relying on the derivatives of mode shapes have attracted increasing attention, examples being the curvature mode shape [30-39], shear-strain gradient [40], and modal Teager-Kaiser energy [41, 42]. As global spatial information of the composite laminate is contained within mode shapes, local changes in the derivatives of mode shapes can characterize the presence, location, and size of damage. For initial damage with slight effect on local stiffness and/or mass in a composite laminate, however, damage-caused changes in derivatives of mode shapes can not only be obscured by fluctuant global trends, but also be overwhelmed by the measurement noise involved in mode shapes that is amplified due to the differentiating operation in the finite difference method. Therefore, damage-caused changes in the derivatives of mode shapes may be barely visible for damage identification.

The “pseudo-force/excitation” approach is one kind of damage identification methods that rely on mode shapes. It is capable of identifying initial damage in beam/plate-like structures because the “pseudo-force/excitation” is determined only by the damage and is free of effect from fluctuant global trends. The concept of “pseudo-force/excitation” is proposed by regarding the damage effect as an equivalent force applying on structural elements bearing damage [43-52]: damage-caused perturbance in local stiffness/mass in the vibration equation of an isotropic beam/plate component is rearranged as an equivalent force (referred to as a “pseudo-force” or “pseudo-excitation”) that exists in the damage region and vanishes elsewhere. Thereby, the presence, location, and size of the initial damage can be characterized by the peak of the pseudo-force/excitation. Representative studies are as follows. Inspired by work in reconstructing the distribution of excitation force applied on beam and plate components [53, 54], Xu et al. [43] developed a novel inverse approach for damage identification by canvassing the local perturbance to equilibrium characteristics of beam components under inspection, by which a through-width notch in an aluminum beam was identified. To deal with noise interference caused by the noise components involved in measured mode shapes, low-pass wavenumber filtering was proposed for denoising. With the same concern about noise interference, Cao et al. [44] transformed the concept of pseudo-force into the wavelet domain, whereby a multi-scale pseudo-force was formulated for crack identification in beam components. The multi-scale nature brought additional benefits to enhance the robustness of detection under noisy measurement conditions. Furthermore, an optimization strategy for evaluating the constant related to frequency and structural and material parameters was integrated into the multi-scale pseudo-force, making the approach suitable for damage identification in beam components with unknown structural and material parameters [45]. Based on

the principle of reconstructing the distribution of interfacial forces and canvassing local perturbance to the structural dynamic equilibrium, Xu et al. [46] established a debonding index together with a hybrid data fusion algorithm for identification of multiple debonding in a steel-reinforced concrete slab. To enhance the noise immunity of the pseudo-excitation approach, Xu et al. [47] established the "weak formulation" of the pseudo-excitation approach by introducing weighted integration, by which multiple cracks were localized in an aluminum beam-like structure. Based on the enhanced pseudo-excitation approach, sub-regions divided from an entire beam component were considered as "virtual" structures undergoing independent vibration, whose "virtual vibration deflections" can be used for locating damage in sub-regions [48]. The enhanced pseudo-excitation approach was further expanded to some beam-type structures whose curvatures/strains are measured instead of displacement [49]: a strategy of reconstruction was proposed to derive the vibration displacements through integration in the spatial domain, making the enhanced pseudo-excitation approach suitable for damage identification using curvature/strain signals. For damage identification in plate-type structures, the enhanced pseudo-excitation approach was expanded to the two-dimensional domain, by which the square and cross-like notches in aluminum plate components with unknown complex boundaries could be identified [50, 51]. Furthermore, the constants related to frequency and structural and material parameters were estimated in a statistical manner, whereby the reliance of the approach on material and structural baseline parameters was eliminated [52]. It is noteworthy that one of the shortcomings of the "pseudo-force" approach is that the excitation is assumed to vanish over the inspected zones. For practical applications, environmental excitations such as wind and thermal loads can also produce fluctuant global trends in the

distribution of the estimated force. In such cases, exciting the inspected structure with stronger intensity to overshadow the environmental effects could be a solution.

Although the pseudo-force/excitation approach is simple and straightforward, its application in damage identification is limited to structural components made of isotropic materials such as steel, aluminum, *etc*., because its nature in a physical sense is based on the vibration of an isotropic element. Therefore, there is a noticeable gap between the pseudo-force/excitation approach and its application in orthotropic and cross-ply composite laminates. To fill this gap, the concept of damage-caused force (DF) is developed from the pseudo-force/excitation, with the objective of identifying initial damage in orthotropic and cross-ply composite laminates with unknown material and structural (i.e., thickness and orientations of plies) parameters. In particular, strategies of isotropization and normalization are integrated into the vibration equation of cross-ply laminates, to deal with the absence of structural and material parameters, respectively.

The rest of the paper is organized as follows. Starting from the vibration equation of orthotropic and cross-ply composite laminates, Section 2 formulates the concept of DF for damage identification in composite laminates without prior knowledge of material and structural parameters. Section 3 numerically verifies the DF concept for identification of a notch/delamination in composite laminates. Section 4 experimentally validates the proposed approach on carbon fiber-reinforced polymer (CFRP) laminates with a notch/delamination. In particular, the CFRP laminates are excited by harmonic waves generated by lead-zirconate-titanate (PZT) piezoelectric actuators, and high-resolution mode shapes are acquired through non-contact measurement using a scanning laser vibrometer (SLV). Section 5 presents concluding remarks.

It is noteworthy that, although commonly used CFRP laminates are used to validate the approach proposed in this study, the approach is established to be generally applicable to other types of fiber-reinforced cross-ply laminates.

2 Identification of damage in composite laminates using damage-caused force

2.1 Equivalent force caused by damage in composite laminates

Consider a fiber-reinforced cross-ply laminate made of 0/90° orientations, M thin plies of which can be regarded as homogeneous and orthotropic. The constitutive (*i.e.*, stress-strain) equations for an element in the *d*th ply can be expressed as [55]

$$\begin{bmatrix} \sigma_x \\ \sigma_y \\ \sigma_{xy} \end{bmatrix}_d = \begin{bmatrix} \bar{Q}_{11} & \bar{Q}_{12} & 0 \\ \bar{Q}_{12} & \bar{Q}_{22} & 0 \\ 0 & 0 & \bar{Q}_{66} \end{bmatrix}_d \begin{bmatrix} \varepsilon_x \\ \varepsilon_y \\ \varepsilon_{xy} \end{bmatrix}_d, \tag{1}$$

where stresses (σ_x, σ_y, and σ_{xy}) and strains (ε_x, ε_y, and ε_{xy}) are in the global coordinates parallel or perpendicular to the fibers, and $\bar{Q}_{ij}$ with $i=1,2,6$ and $j=1,2,6$ are the corresponding material coefficients, as can be found in Ref. [55].

By integrating stresses over the cross-section of the laminate, we obtain the bending moments M_x and M_y and the twisting moment M_{xy}:

$$\begin{bmatrix} M_x \\ M_y \\ M_{xy} \end{bmatrix} = \begin{bmatrix} D_{11} & D_{12} & 0 \\ D_{12} & D_{22} & 0 \\ 0 & 0 & D_{66} \end{bmatrix} \begin{bmatrix} \kappa_x \\ \kappa_y \\ 2\kappa_{xy} \end{bmatrix}, \tag{2}$$

where $D_{ij} = \frac{1}{3}\sum_{d=1}^{M} \bar{Q}_{ij}^{(d)} (z_d^3 - z_{d-1}^3)$ are stiffness coefficients ply-wisely integrated over the thickness, and z^k is the distance from the middle surface to the surface of the *d*th ply having the furthest *z*-coordinate. $\kappa_x = \frac{\partial^2 w}{\partial x^2}$ and $\kappa_y = \frac{\partial^2 w}{\partial y^2}$ are the curvatures, and $\kappa_{xy} = \frac{\partial^2 w}{\partial x \partial y}$ is the twist in the midsurface.

The out-of-plane vibration equation of thin composite laminates subject to transverse excitation can be written as

$$D_{11}\frac{\partial^4 w}{\partial x^4}+2(D_{12}+2D_{66})\frac{\partial^4 w}{\partial x^2\partial y^2}+D_{22}\frac{\partial^4 w}{\partial y^4}+\bar{\rho}\frac{\partial^2 w}{\partial t^2}+c\frac{\partial w}{\partial t}=q, \tag{3}$$

where $w(x,y,t)$ is the out-of-plane displacement, $\bar{\rho}=\sum_{d=1}^{M}\rho^{(d)}(z_d-z_{d-1})$ is the average mass density of the laminated plate per unit area of the midsurface with $\rho^{(d)}$ being the density of the dth lamina per unit volume, c is the damping coefficient, $q(x,y)$ is the transverse excitation applying on the surface of the laminate. It is noteworthy that Eq. (3) is only suitable for thin laminated composites constructed with very thin layers of lamina. For the vibration equation of thick composite laminates, shear deformation and rotary inertia should be taken into consideration, following Mindlin's theory [55].

When local damage like a notch or a delamination occurs in a composite laminate, its local stiffness and/or mass will be reduced in the damage region [56]. Considering a composite laminate bearing local damage in a region denoted as Ω, the stiffness coefficients $D_{ij}(x,y)$ and average mass density $\bar{\rho}(x,y)$ of the laminate can be represented as

$$D_{ij}(x,y)=\begin{cases}D_{ij}^{I} & x,y\notin\Omega\\ D_{ij}^{D} & x,y\in\Omega\end{cases}, \tag{4a}$$

$$\bar{\rho}(x,y)=\begin{cases}\bar{\rho}^{I} & x,y\notin\Omega\\ \bar{\rho}^{D} & x,y\in\Omega\end{cases}, \tag{4b}$$

where superscripts I and D indicate the intact and damaged statuses, respectively.

By substituting Eq. (4) into Eq. (3) and rearranging Eq. (3), we obtain

$$D_{11}^{I}\frac{\partial^4 w}{\partial x^4}+2(D_{12}^{I}+2D_{66}^{I})\frac{\partial^4 w}{\partial x^2\partial y^2}+D_{22}^{I}\frac{\partial^4 w}{\partial y^4}+\bar{\rho}^{I}\frac{\partial^2 w}{\partial t^2}+c\frac{\partial w}{\partial t}=q+f_{DF}, \tag{5}$$

where f_{DF} is the equivalent transverse force caused by the damage, defined as the DF, which exists only in the damage region and vanishes elsewhere:

$$f_{DF}=\begin{cases} 0 & x,y\notin\Omega \\ \Delta\mathbf{D}\cdot\boldsymbol{\Theta}(w)+\Delta\bar{\rho}\dfrac{\partial^2 w}{\partial t^2} & x,y\in\Omega \end{cases}, \tag{6}$$

with stiffness change vector $\Delta\mathbf{D}=(D_{11}^{I}-D_{11}^{D},(D_{12}^{I}+2D_{66}^{I})-(D_{12}^{D}+2D_{66}^{D}),D_{22}^{I}-D_{22}^{D})$, density change $\Delta\bar{\rho}=\bar{\rho}^{I}-\bar{\rho}^{D}$, and $\boldsymbol{\Theta}(\square)=(\dfrac{\partial^4}{\partial x^4},\dfrac{2\partial^4}{\partial x^2\partial y^2},\dfrac{\partial^4}{\partial y^4})$.

Regarding the elements of the composite laminate bearing no transverse excitation, *i.e.*, $q=0$, Eq. (5) becomes

$$D_{11}^{I}\frac{\partial^4 w}{\partial x^4}+2(D_{12}^{I}+2D_{66}^{I})\frac{\partial^4 w}{\partial x^2\partial y^2}+D_{22}^{I}\frac{\partial^4 w}{\partial y^4}+\bar{\rho}^{I}\frac{\partial^2 w}{\partial t^2}+c\frac{\partial w}{\partial t}=f_{DF}. \tag{7}$$

The displacement $w(x,y,t)$ can be further expressed as $W(x,y)e^{-i\omega t}$ when $W(x,y)$ represents a mode shape associated with the corresponding natural frequency ω and i denotes the imaginary unit. Substituting $w=We^{-i\omega t}$ into Eq. (7), we have

$$D_{11}^{I}\frac{\partial^4 W}{\partial x^4}+2(D_{12}^{I}+2D_{66}^{I})\frac{\partial^4 W}{\partial x^2\partial y^2}+D_{22}^{I}\frac{\partial^4 W}{\partial y^4}-\omega^2\bar{\rho}^{I}W-ic\omega W=F_{DF}, \tag{8}$$

where $F_{DF}=\begin{cases} 0 & x,y\notin\Omega \\ \Delta\mathbf{D}\cdot\boldsymbol{\Theta}(W)-\omega^2\Delta\bar{\rho}W & x,y\in\Omega \end{cases}$.

As can be seen from Eq. (8), for a composite laminate bearing local damage, the DF appears only in the damage region and vanishes in other places. Thereby, the principle of damage identification in composite laminates using the DF is established: the occurrence of damage can be indicated by the appearance of a sharply-rising peak in the DF; furthermore, the location and size of the damage can be also quantitatively characterized by the damage-caused peak.

2.2 Evaluation of damage index without material and structural parameters

Although the principle of damage identification using the DF is simple and straightforward, accurate baseline information, including material and structural parameters of the composite laminates, needs to be precognitive, which impairs its application to real-world composite structures whose material and structural parameters are unknown in most scenarios. When dealing with unknown material and structural parameters in Eq. (8), a strategy of isotropization is proposed by introducing a virtual isotropic bending stiffness D^I (under a structurally intact status) into Eq. (8); then a strategy of normalization is proposed by dividing D^I on both sides of the equation, so that we have

$$\frac{\partial^4 W}{\partial x^4}+2\frac{\partial^4 W}{\partial x^2\partial y^2}+\frac{\partial^4 W}{\partial y^4}-\lambda^4 W=\tilde{F}_{DF}+\tilde{q}, \tag{9}$$

where $\lambda^4=\frac{\omega^2\overline{\rho}^I}{D^I}$ is the constant related to the frequency and structural and material parameters, $\tilde{F}_{DF}=\frac{F_{DF}}{D^I}$ is the normalized DF, $\tilde{q}=\Delta\tilde{\mathbf{D}}\cdot\boldsymbol{\Theta}(W)$ is an additional transverse force caused by the isotropization that applies on entire the laminate with $\Delta\tilde{\mathbf{D}}=(1-\frac{D_{11}^I}{D^I},1-\frac{D_{12}^I}{D^I}-2\frac{D_{66}^I}{D^I},1-\frac{D_{22}^I}{D^I})$. According to Eq. (9), the normalized DF contains components of the elastic force $\tilde{F}_{EF}$, inertia force $\tilde{F}_{IF}$, and isotropization-caused force $\tilde{F}_{ISOF}$:

$$\tilde{F}_{DF}=\tilde{F}_{EF}+\tilde{F}_{IF}+\tilde{F}_{ISOF}, \tag{10}$$

where $\tilde{F}_{EF}=\frac{\partial^4 W}{\partial x^4}+2\frac{\partial^4 W}{\partial x^2\partial y^2}+\frac{\partial^4 W}{\partial y^4}=\nabla^4 W$ with $\nabla^4=\nabla^2(\nabla^2)$, $\tilde{F}_{IF}=-\lambda^4 W$, $\tilde{F}_{ISOF}=-\tilde{q}$.

Among the three force components in Eq. (10), it is reasonable to assume that the isotropization-caused force is much weaker than the sum of other two force components, *i.e.*, $\tilde{F}_{ISOF}\ll\tilde{F}_{EF}+\tilde{F}_{IF}$, because the isotropization-caused force reflects the difference the between isotropic and orthotropic materials in modelling plies. Therefore, the

normalized DF $\tilde{F}_{DF}$ can be approximately expressed as the sum of the elastic force $\tilde{F}_{EF}$ and the inertia force $\tilde{F}_{IF}$, *i.e.*, $\tilde{F}_{DF} \approx \tilde{F}_{EF} + \tilde{F}_{IF}$. In this situation, the amplitude of the damage-caused peak in the normalized DF is presumed to be much greater than the difference caused the isotropization-caused force, so that the damage can still be clearly characterized by the damage-caused peak. This assumption is proved in numerical and experimental cases in Sections 3 and 4. Therefore, the damage index, denoted as DI, can be established using the approximation of the normalized DF without the isotropization-caused force:

$$DI = \tilde{F}_{DF} \approx \tilde{F}_{EF} + \tilde{F}_{IF} = \nabla^4 W - \lambda^4 W, \tag{11}$$

in which fourth derivatives that constitute $\nabla^4 W$ can be calculated by the finite difference method [54]:

$$\begin{aligned} \frac{\partial^4 W}{\partial x^4}[x,y] = \frac{1}{h_x^4}(&W[x-2h_x,y] - 4W[x-h_x,y] + 6W[x,y] \\ &-4W[x+h_x,y] + W[x+2h_x,y]), \end{aligned} \tag{12a}$$

$$\begin{aligned} \frac{\partial^4 W}{\partial x^2 \partial y^2}[x,y] = \frac{1}{h_x^2 h_y^2}(&W[x-h_x,y-h_y] - 2W[x-h_x,y] + W[x-h_x,y+h_y] \\ &- 2W[x,y-h_y] + 4W[x,y] - 2W[x,y+h_y] \\ &+ W[x+h_x,y-h_y] - 2W[x+h_x,y] + W[x+h_x,y+h_y]), \end{aligned} \tag{12b}$$

$$\begin{aligned} \frac{\partial^4 W}{\partial y^4}[x,y] = \frac{1}{h_y^4}(&W[x,y-2h_y] - 4W[x,y-h_y] + 6W[x,y] \\ &-4W[x,y+h_y] + W[x,y+2h_y]). \end{aligned} \tag{12c}$$

As the material and structural parameters of the composite laminate are unknown, the constant λ^4 cannot be directly obtained. Addressing this problem, in this study, λ^4 is evaluated in a statistical manner by calculating values of λ^4 for each measurement point, which is termed a point-wise constant that is related to the frequency and structural and material parameters, denoted as $\lambda^4[x,y]$. As DI given

in Eq. (11) vanishes in the intact region of the composite laminate ($x, y \notin \Omega$), $\lambda^4[x, y]$ can be alternatively calculated using the measured mode shape:

$$\lambda^4[x, y] = \nabla^4 W / W. \tag{13}$$

The point-wise constant $\lambda^4[x, y]$ with maximum probability will be regarded as the constant λ^4; in turn, DI can be obtained by Eq. (11). Meanwhile, as the constant λ^4 can be determined directly from the measured mode shape, excitation parameters such as location, amplitude, and frequency can be unknown when calculating DI. Therefore, not only material and structural parameters can be absent, but also excitation parameters can be unknown for the approach.

It is noteworthy that the approach is independent of the virtual bending stiffness D^I that is introduced into Eq. (9), and requires only the measured mode shape. Therefore, the approach proposed in this study for identification of damage in composite laminates is baseline-free, which means that no material or structural parameters are required.

2.3 Multi-resolution damage index relying on damage-caused force

As noise components are inevitably involved in measured mode shapes and are amplified by the differentiating operation in Eq. (12), the actual damage-caused peaks in the DF could be masked by intense noise interference. To deal with noise contamination in the measured mode shapes, the multi-resolution analysis (MRA) is integrated into the damage index to form a multi-resolution damage index with higher noise robustness. The 2D wavelet function $\psi^v(x, y)$ ($v = 1, 2, 3$) can be formulated as the product of the 1D wavelet and scaling functions [57, 58]:

$$\psi^1(x, y) = \phi(x)\psi(y), \tag{14a}$$

$$\psi^2(x,y)=\psi(x)\phi(y), \tag{14b}$$

$$\psi^3(x,y)=\psi(x)\psi(y), \tag{14c}$$

$$\phi(x,y)=\phi(x)\phi(y), \tag{14d}$$

where $\psi(x)$ and $\psi(y)$ are 1D wavelet functions, $\phi(x)$ and $\phi(y)$ are 1D scaling functions. By dilating and translating the mother wavelet and scaling functions, wavelet and scaling functions at MRA levels j can be obtained:

$$\psi^v_{j,k,l}(x,y)=2^{-j}\psi^v(2^{-j}x-k,2^{-j}y-l); \qquad j,k,l\in\mathbb{Z}, \tag{15a}$$

$$\phi_{j,k,l}(x,y)=2^{-j}\phi(2^{-j}x-k,2^{-j}y-l); \qquad j,k,l\in\mathbb{Z}. \tag{15b}$$

The discretized signal of a mode shape W can be decomposed into multiple levels:

$$W=\sum_j W_j. \tag{16}$$

Correspondingly, subspaces $\mathbf{W}_j$ of $\mathbf{L}^2(\mathbb{Z})$ are spanned by $\psi^v_{j,k,l}$, which are orthogonal to each other; on the other hand, $\mathbf{V}_j$ can be spanned by $\psi^v_{i,k,l}$ for $i>j$, which leads to $\mathbf{V}_{j-1}=\mathbf{V}_j\oplus\mathbf{W}_j$:

$$\mathbf{W}_j=\text{span}(\psi^v_{j,k,l}: j,k,l\in\mathbb{Z}), \tag{17a}$$

$$\mathbf{V}_j=\text{span}(\psi^v_{i,k,l}: i,k,l\in\mathbb{Z}, i>j). \tag{17b}$$

Thus, $\mathbf{L}^2(\mathbb{Z})$ can be decomposed into:

$$\mathbf{L}^2(\mathbb{Z})=\mathbf{V}_j\oplus\mathbf{W}_j\oplus\cdots\oplus\mathbf{W}_1\oplus\mathbf{W}_0\oplus\mathbf{W}_{-1}\oplus\mathbf{W}_{-2}\oplus\cdots \tag{18}$$

Accordingly, W in $\mathbf{V}_0$ with the finest resolution can be decomposed into the approximation A_N in $\mathbf{V}_N$ and the details D^v_j in $\mathbf{W}_j$:

$$W[x,y]=A_N[x,y]+\sum_{v=1}^{3}\sum_{j=1}^{N}D^v_j[x,y], \tag{19}$$

where A_N and D^v_j can be calculated by the discrete wavelet transform (DWT):

$$A_N = \sum_{v=1}^{3} \sum_{i>j} \sum_{k} \sum_{l} a_{i,k,l}^{v} \psi_{i,k,l}^{v}, \tag{20a}$$

$$D_j^v = \sum_{k} \sum_{l} a_{j,k,l}^{v} \psi_{j,k,l}^{v}, \tag{20b}$$

with wavelet transform coefficients $a_{i,k,l}^{v}$ being calculated by the inner product of W and $\psi_{j,k,l}^{v}$:

$$a_{i,k,l}^{v} = \left\langle W, \psi_{i,k,l}^{v} \right\rangle. \tag{21}$$

Among the Daubechies wavelet family, the well-known Db 1 wavelet, also called the Haar wavelet, is employed in this study for its simplicity and operability for engineers:

$$\phi(x) = \begin{cases} 1 & 0 \le x < 1, \\ 0 & \text{otherwise}, \end{cases} \tag{22a}$$

$$\psi(x) = \begin{cases} 1 & 0 \le x < 1/2, \\ -1 & 1/2 \le x < 1, \\ 0 & \text{otherwise}. \end{cases} \tag{22b}$$

As per the MRA above, the damage index DI given in Eq. (11) can be enhanced to form the multi-resolution damage index, denoted as $MRDI$, by replacing the noisy W with the noise-free A_N:

$$MRDI = \nabla^4 A_N - \lambda^4 A_N, \tag{23}$$

in which λ^4 can be determined by $\lambda_N^4[x, y]$ with the maximum probability:

$$\lambda_N^4[x, y] = \nabla^4 A_N / A_N, \tag{24}$$

in which $\lambda_N^4[x, y]$ is termed the point-wise constant at MRA level of N. The satisficing level of $MRDI$ can be determined by gradually increasing the level until noise interference in the $MRDI$ is eliminated. Meanwhile, the damage-caused peak is retained to clearly characterize the damage. It is noteworthy that other types of high-order wavelets in the Daubechies wavelet family can also be employed for the MRA.

Thereby, the multi-resolution damage index is suitable for damage identification in composite laminates in noisy conditions.

3 Numerical verification

Numerical simulation by the finite element (FE) method is used to verify the capability of the multi-resolution damage index for damage identification in composite laminates without prior knowledge of material and structural parameters.

3.1 FE modeling of composite laminates

An 8-layer CFRP symmetric cross-ply laminate made of 0/90° orientations is considered as the specimen for numerical simulation, its dimensions being 500 mm × 500 mm × 3 mm in the *x*-, *y*-, and *z*-directions, respectively. The laminate is modeled by the FE software ANSYS with eight-node hexahedral elements with the dimensions 5 mm × 5 mm × 0.375 mm in the *x*-, *y*-, and *z*-directions, respectively. The elastic modulus in 0º and 90º are E_{11} 92 GPa and E_{22} 8 GPa, respectively; in-plane shear modulus, Poisson's ratio, and material density are G_{12} 2.9 GPa, ν_{12} 0.33, and ρ 1400 Kgm^{-3}, respectively. Introduced into the model is a square damage centered at *x*=150 mm and *y*=350 mm, spanning from *x*=140 mm to 160 mm and from *y*=340 mm to 360 mm (illustrated in Fig. 1). Without loss of generality, by introducing the dimensionless coordinates $\zeta = \frac{x}{500}$ and $\eta = \frac{y}{500}$, the damage is centered at $\zeta = 0.3$ and $\eta = 0.7$, spanning from 0.28 to 0.32 in ζ, and from 0.68 to 0.72 in η.

For validation of the proposed approach for damage identification in composite laminates, damage instances in the FE model are modeled as a notch and a delamination. The first type of damage is modeled as a notch by reducing one quarter of thickness from the front surface of the laminate. The second type of damage is modeled as a delamination by inserting a non-thickness interface between the interfaces of the second

and third plies; on the non-thickness interface of the delamination, the coincident nodes in adjacent but separated elements are distributed.

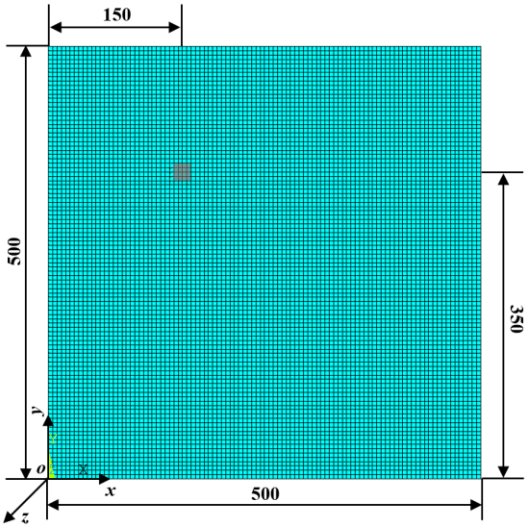

Fig. 1. FE model of CFRP laminate with square damage (dimensions in millimeters).

3.2 Numerical results

Equation (13) indicates that $\lambda^4[x,y]$ is only determined by the measured mode shape and is independent of materials, boundary conditions, and the mode selected. However, uncertainties can be introduced by numerical calculation as expressed in Eq. (12), with the result that the λ^4 defined in Eq. (9) cannot be a constant for all the measurement points in the laminate. Addressing this problem, in this study, λ^4 is evaluated in a statistical manner: a point-wise constant $\lambda^4[x,y]$ for each measurement point is calculated, among which the $\lambda^4[x,y]$ with the maximum probability can be regarded as λ^4. To exclude any effect of damage, intact models with different materials and boundary conditions are employed to investigate the statistical distribution of $\lambda^4[x,y]$. By modal analysis, out-of-plane mode shapes (in the z-direction) of the intact FE model can be extracted from the out-of-plane displacements of 101 × 101 nodes on the back surface of the laminate; for generality, each mode shape is of a unit maximum amplitude. As low-order modes are insensitive to incipient damage [29], high-order modes are

considered in this study. Figures 2(a) and (b) show the 26th and the 66th mode shapes of intact aluminum and CFRP laminated plates with the boundary conditions C-F-F-F ("C" for clamped and "F" for free) and F-F-F-F, respectively. Correspondingly, $\lambda^4[x,y]$ can be calculated by Eqs. (12) and (13), whose statistical distributions over 1000 uniform sections are shown in Figs. 3(a) and (b), respectively. It can be found that, due to calculation-induced uncertainties, the count distribution of $\lambda^4[x,y]$ is narrow bell-shaped. Thereby, $\lambda^4[x,y]$ with the maximum count (probability) can be regarded as λ^4.

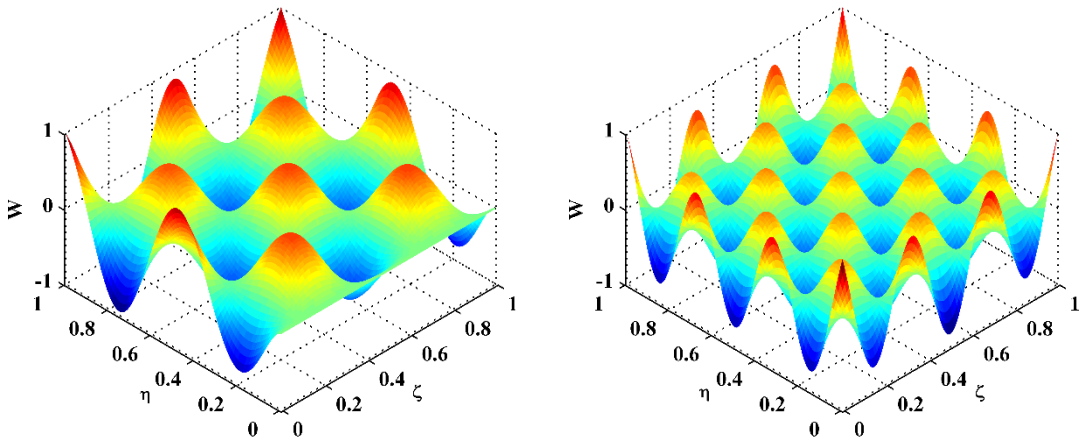

(a) (b)

Fig. 2. Mode shapes of intact (a) aluminum plate and (b) CFRP laminated plate.

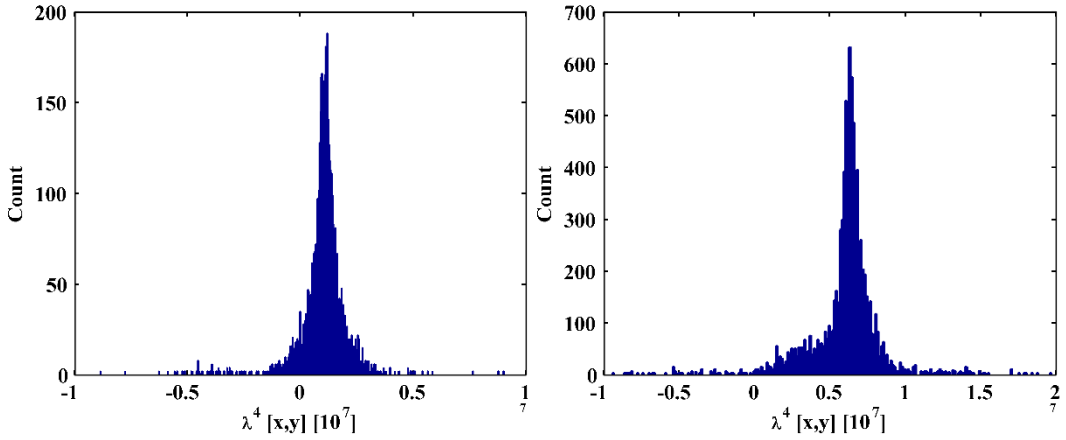

(a) (b)

Fig. 3. Statistical distributions of point-wise constants for intact (a) aluminum plate and (b) CFRP laminated plate.

After introduction of the damage into the CFRP laminate model, mode shapes can be obtained by modal analysis in ANSYS. To increase the resolution of the mode shapes for better visualization of damage identification, interpolation is implemented to increase the dimensions of the mode shapes from the 101 × 101 to 401 × 401 by interpolation at sampling intervals of 1.25 mm in both directions. The 66th mode shapes of the CFRP laminates with a notch and a delamination are shown in Figs. 4(a) and 5(a), respectively. Correspondingly, point-wise constants $\lambda^4[x,y]$ are calculated by Eq. (13). Count distributions of point-wise $\lambda^4[x,y]$ are shown in Figs. 4(b) and 5(b), from which the constants λ^4 can be determined by corresponding $\lambda^4[x,y]$ with the maximum counts. Thereby, λ^4 for the CFRP laminate models with a notch and a delamination are determined as 2.95×10^4 and 2.23×10^4, respectively.

From Eq. (11), damage indices DI for the CFRP laminate models with a notch and a delamination are obtained from the corresponding mode shapes and are shown in Figs. 6(a) and (c), respectively. In each DI, a peak rises sharply in the square damage region and almost vanishes in other places. Thereby, the presence of the damage is evidently manifested. In their planforms as shown in Figs. 6(b) and (d), damage locations and sizes are well characterized: the identified notch and delamination are centered at $\zeta = 0.3$ and $\eta = 0.7$, spanning from 0.28 to 0.32 in ζ, and from 0.68 to 0.72 in η, corresponding to the actual damage regions whose outlines are marked in white in Figs. 6(b) and (d).

It is worthy of note that the DI shown in Fig. 6 also verify the assumption made in Eq. (11): the isotropization-caused force is much weaker than the sum of the other

two force components. Therefore, it is reasonable to ignore the isotropization-caused force when the DI is formulated using the DF.

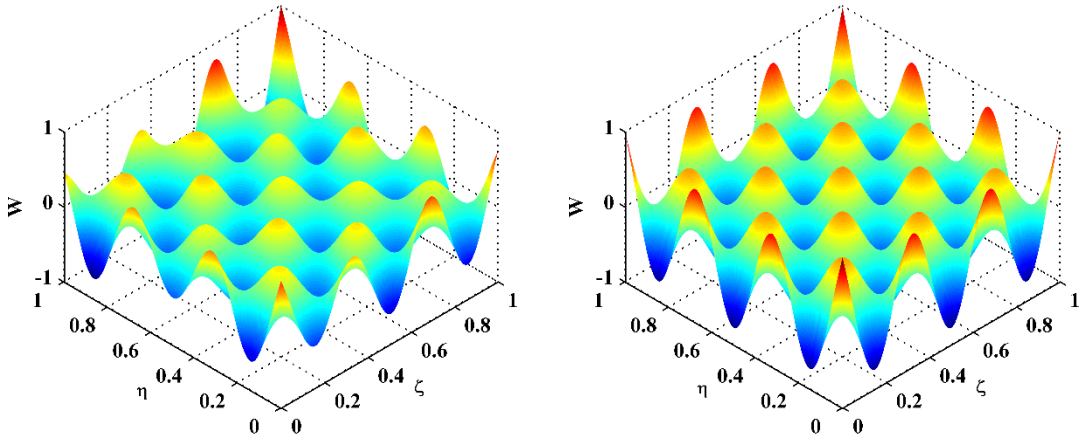

(a) (b)

Fig. 4. Mode shapes of CFRP laminates with (a) a notch and (b) a delamination.

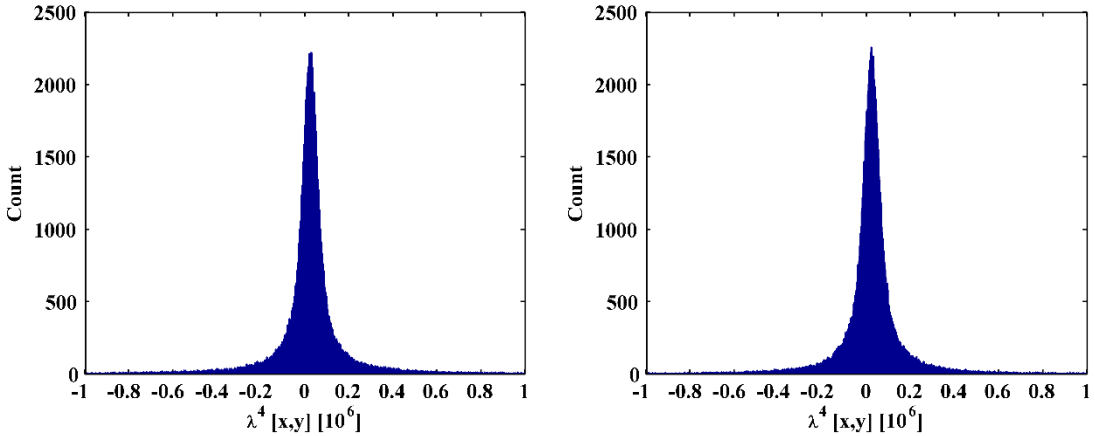

(a) (b)

Fig. 5. Statistical distributions of point-wise constants for CFRP laminates with (a) a notch and (b) a delamination.

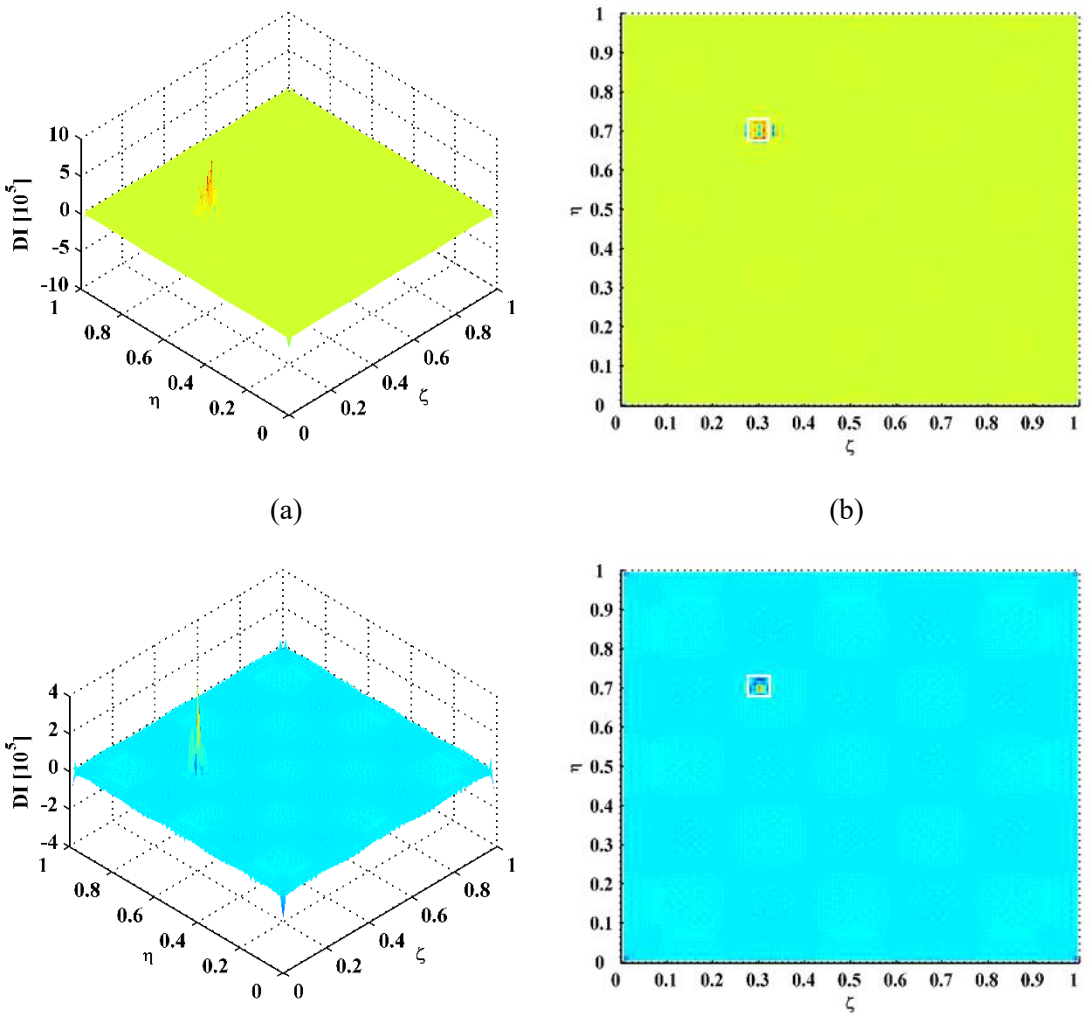

Fig. 6. Damage indices for CFRP laminate with (a) a notch and (c) a delamination, with their planforms (b) and (d), respectively.

In real scenarios of measuring mode shapes with dense spatial samplings, noise components are inevitably involved in the measured mode shapes. With this concern, Gaussian white noise is incorporated into the mode shapes to simulate environmental noise effect, by which noisy mode shapes with the signal-to-noise ratio (SNR) of 60 dB are produced. The corresponding $\nabla^4 W$ are obtained by Eq. (12) and shown in Fig. 7, in which noise interference dominates and hinders further calculation of the DI. The reason for the noise interference is that if the spatial interval of the mode shape is small,

the fourth-order derivatives of the mode shape can become instable due to the amplified noise components. To eliminate noise interference, multi-resolution damage indices $MRDI$ formulated in Section 3 are obtained by Eq. (23). By means of a gradual increase in the MRA level, the approximations A_{40} at the MRA level of 40 can be obtained, as shown in Fig. (8). By Eq. (24), the corresponding $\lambda_{40}^4[x,y]$ can be calculated, as shown in Fig. (9) distributed in 1000 uniform sections, among which the $\lambda_{40}^4[x,y]$ with the maximum counts are 2.95×10^4 and 2.23×10^4 (exactly the same as those in noise-free situations) for the CFRP laminates with a notch and a delamination, respectively. Then, $MRDI$ are obtained by Eq. (23) and shown in Fig. 10. It can be seen from Fig. 8 that noise interference is basically eliminated. Synchronously, damage-caused peaks appear clearly in the notch region (Fig. 10(a)) and the delamination region (Fig. 10(c)), respectively. Accordingly, in their planforms shown in Figs. 10(b) and (d), the locations of the damage-caused peaks are in good agreement with the actual regions of the notch and the delamination, whose outlines are marked in white, respectively. It should be noted that values of $MRDI$ near the boundaries are made to vanish, in order to remove the boundary distortion effect in the DWT [41].

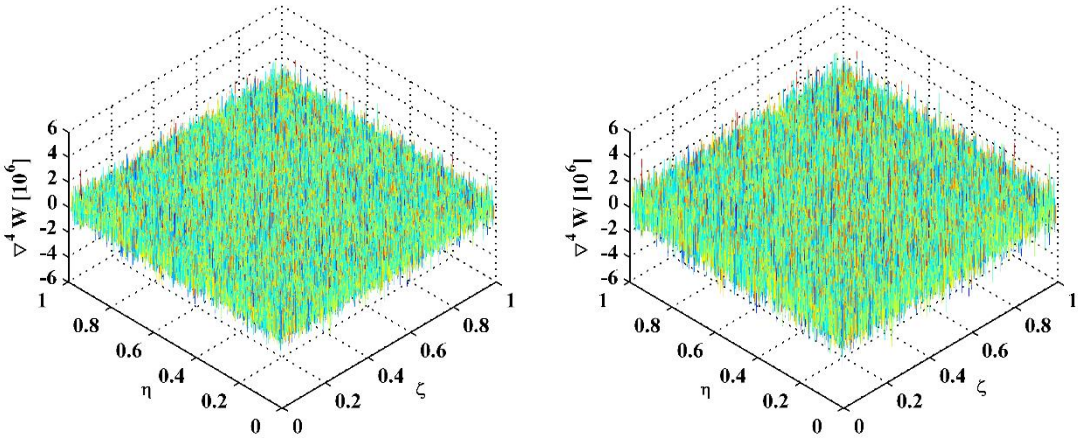

(a) (b)

Fig. 7. $\nabla^4 W$ for CFRP laminates with (a) a notch and (b) a delamination in noisy conditions.

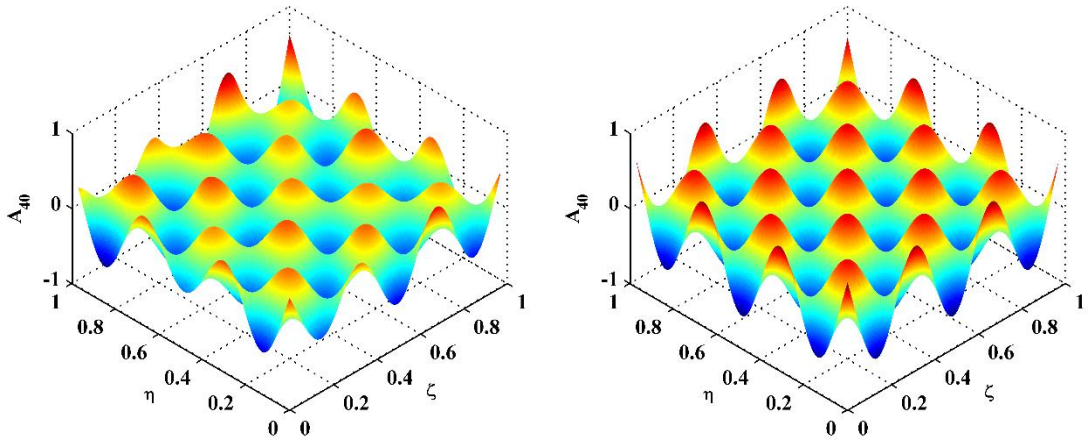

Fig. 8. Approximations for CFRP laminates with (a) a notch and (b) a delamination.

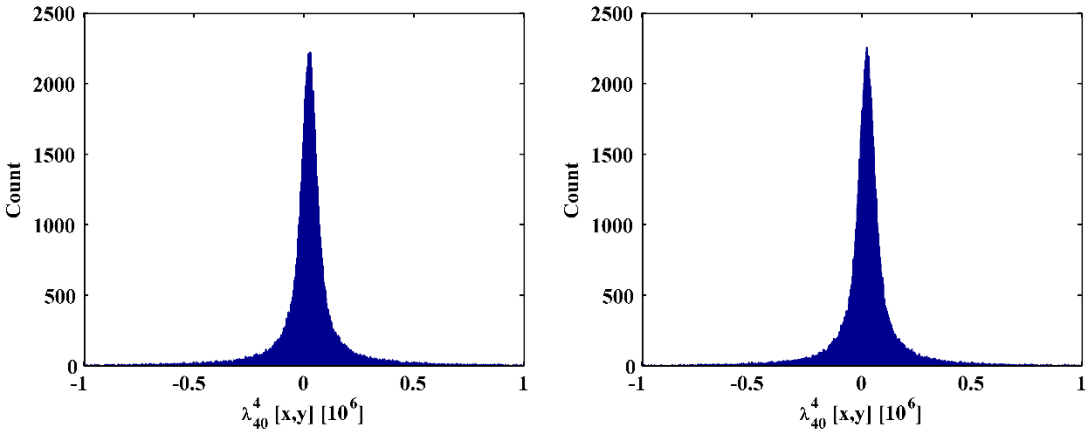

Fig. 9. Statistical distributions of point-wise constant for CFRP laminates with (a) a notch and (b) a delamination.

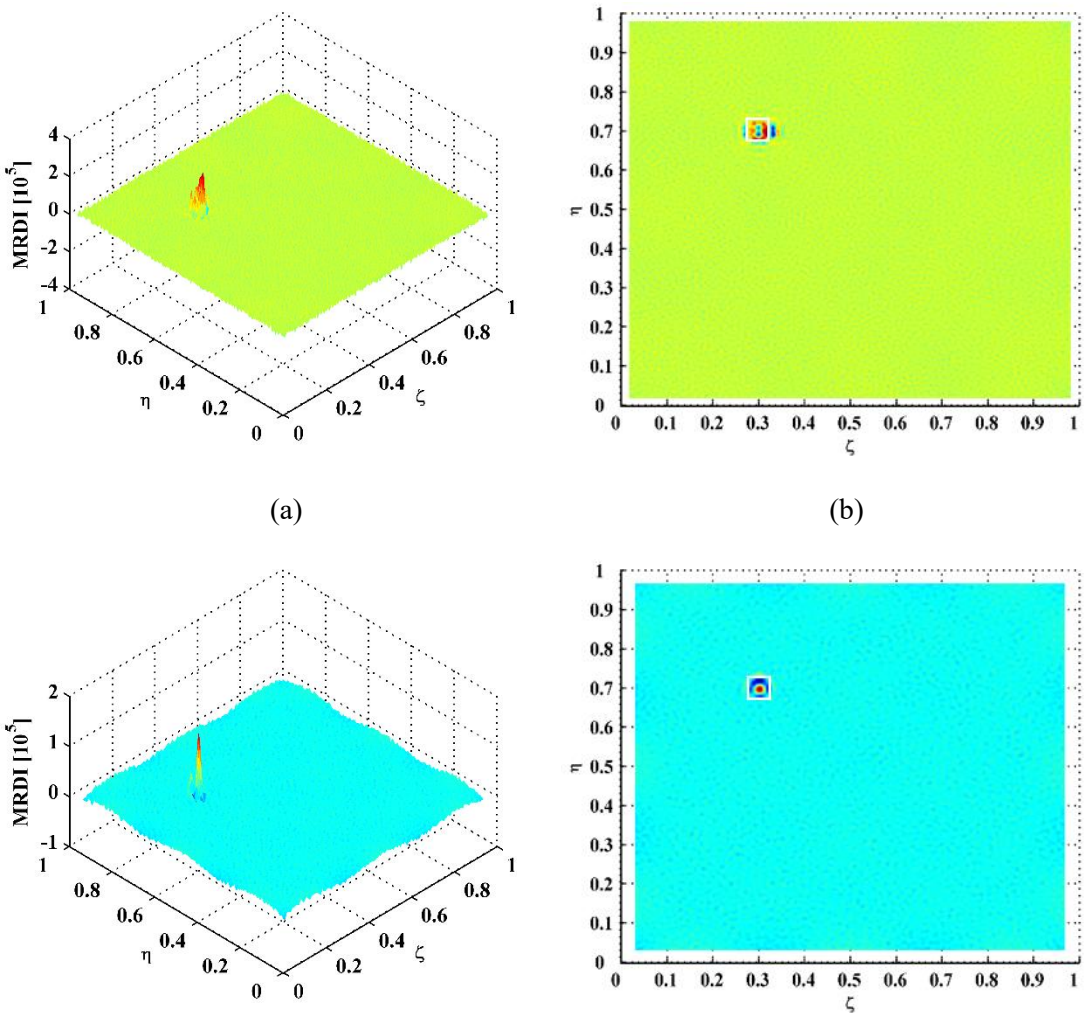

Fig. 10. Multi-resolution damage indices for CFRP laminates with (a) a notch and (c) a delamination, with their planforms (b) and (d), in noisy conditions.

To explore the noise tolerance of the multi-resolution damage index, noisier levels with lower SNRs of 70 dB and 60 dB are considered, respectively. For the scenario with SNR 70 dB, when the DWT level is increased to 50, it can be seen from Figs. 11(a) and (c) that the damage-caused peaks in *MRDI* clearly designate the presence and locations of the notch and the delamination, respectively. When the noise intensity is increased to SNR 60 dB, *MRDI* become noisier but their damage-caused peaks can still clearly identify the notch (Fig. 11(b)) and the delamination (Fig. 11(d)) by

increasing the MRA level to 60. However, for even noisier mode shapes with lower SNRs, *MRDI* will become too ambiguous to indicate any damage feature, even at higher MRA levels. Thus, SNR 60 dB can be regarded as the noise tolerance of the proposed approach in this numerical case.

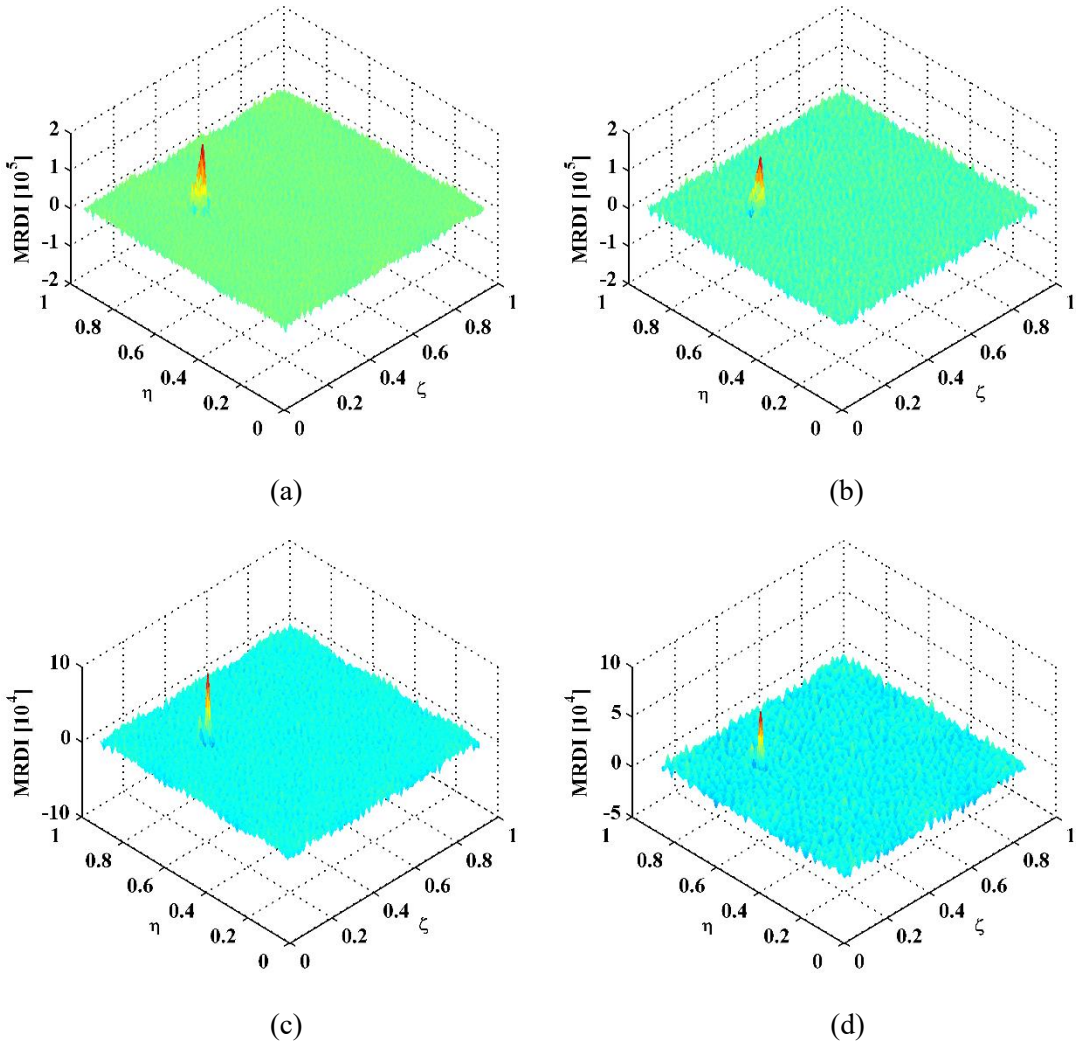

Fig. 11. Multi-resolution damage indices for CFRP laminates with a notch ((a) and (b)) and a delamination((c) and (d)) in noisier conditions.

4 Experimental validation

The applicability of the multi-resolution damage index is investigated for damage identification in composite laminates, whose material and structural parameters are absent.

4.1 Experimental set-up

Two CFRP (GG204P IMP503 42) symmetric cross-ply laminates made of 0/90° orientations are taken as specimens. The first CFRP laminate specimen bears a square notch on the front surface, as shown in Fig. 12(a). The dimensions of the first CFRP laminate specimen are 400 mm × 400 mm × 3 mm in the *x*-, *y*-, and *z*-directions, respectively. The square notch (20 mm × 20 mm) was manufactured by digging through the first and second plies from the front surface of the laminate. On the back surface of the laminate, the measurement zone spans from 20 mm to 380 mm and from 20 mm to 380 mm in the *x*- and *y*-directions, respectively. The notch is centered at *x*=290 mm and *y*=290 mm, spanning from 280 mm to 300 mm and from 280 mm to 300 mm in the *x*- and *y*-directions, respectively. In the dimensionless coordinates, the delamination is centered at $\zeta = 0.75$ and $\eta = 0.75$, spanning from 0.722 to 0.778 in ζ, and from 0.722 to 0.778 in η in the measurement zone. At the geometrical center of the front surface, a circular PZT piezoelectric actuator with the diameter of 10 mm is placed to generate harmonic waves to excite the CFRP laminate. Synchronously, a SLV (Polytec PSV-400) is employed to scan the entire back surface covered by reflection tapes with 271 × 271 densely-distributed measurement points at sampling intervals of about 1.33 mm in both directions. Velocity responses of 271 × 271 measurement points in the measurement zone are acquired by the SLV, whereby the operating deflection shapes (ODSs) at the excitation frequency can be obtained. The optimal sampling interval is determined by gradually reducing the size of sampling interval until it matches the size of the identified damage. To accurately characterize the damage, the size of the sampling interval should be no greater than the size of the damage. On the other hand, over-dense sampling will be time-consuming for measurement. The experimental set-up is shown in Fig. 13.

The second CFRP laminate specimen bears a square delamination between the second and third plies (the front surface belongs to the first ply), as shown in Fig. 12(b). The dimensions of the second CFRP laminate specimen are 500 mm × 500 mm × 3 mm in the *x*-, *y*-, and *z*-directions, respectively. To manufacture a delamination, a square Teflon sheet (15 mm × 15 mm) was inserted between the interfaces of the second and third plies when the CFRP laminate was fabricated. The measurement zone is expanded and almost covers the back surface of the laminate. The delamination is centered at *x*=125 mm and *y*=375 mm, spanning from 117.5 mm to 132.5 mm and from 367.5 mm to 382.5 mm in the *x*- and *y*-directions, respectively. In the dimensionless coordinates, the delamination is centered at $\zeta = 0.75$ and $\eta = 0.75$, spanning from 0.235 to 0.265 in ζ, and from 0.735 to 0.765 in η, respectively, in the measurement zone. In this case, the circular PZT piezoelectric actuator is moved to the lower left corner on the front surface to excite the CFRP laminate by generating harmonic waves. Synchronously, the SLV is employed to scan the measurement zone on the back surface covered by reflection tapes with 375 × 375 densely-distributed measurement points at sampling intervals of about 1.33 mm in both directions. ODSs can be acquired from the velocity responses of 375 × 375 measurement points.

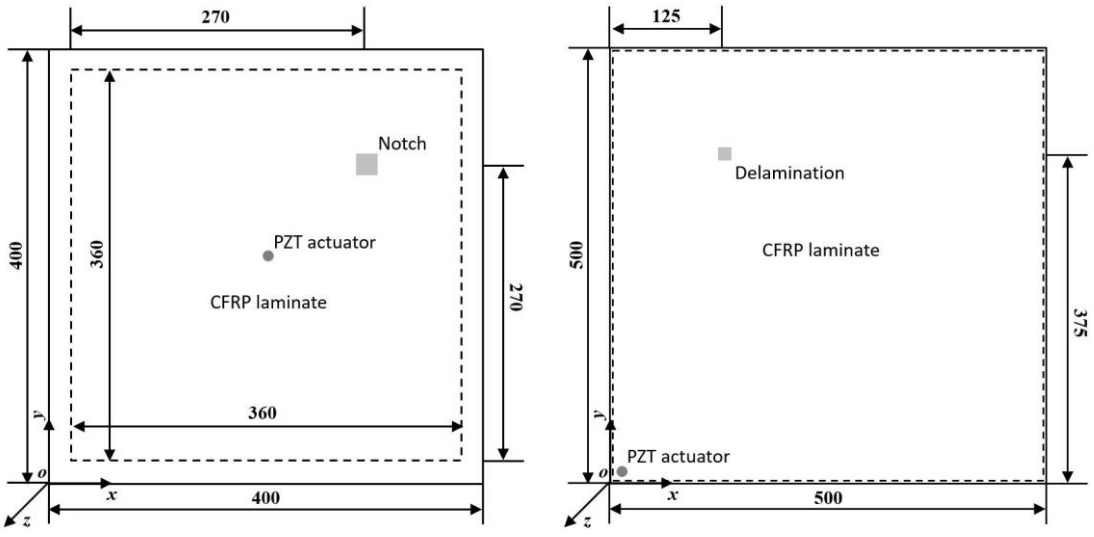

(a) (b)

Fig. 12. Diagrams of CFRP laminates with (a) a notch and (b) a delamination (dimensions in millimeters).

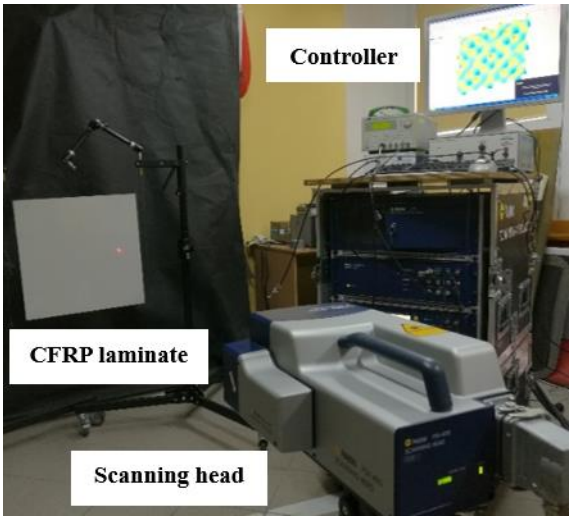

Fig. 13. Experimental specimen and set-up.

4.2 Experimental results

For the CFRP specimen with a notch, a natural frequency at 388.1 Hz is selected after modal analysis over a broad frequency range [59]. Subject to harmonic excitation at that natural frequency, the ODS acquired by the SLV approximates the mode shape associated with the corresponding natural frequency [60], as shown in Fig. 14(a) with a unit maximum amplitude. To eliminate the noise components contained in the mode shape, the mode shape is decomposed into its approximation and details at the level of 60. The point-wise constants $\lambda_{60}^{4}[x,y]$ are calculated by Eq. (24), as shown in Fig. 14(b). After sorting $\lambda_{60}^{4}[x,y]$ into 1000 uniform sections, $\lambda_{60}^{4}[x,y]$ being 3.63×10^{6} with the maximum count can be regarded as the constant λ^{4}. Then, the multi-resolution damage index $MRDI$ is obtained by Eq. (23) and shown in Fig. 15, where a damage-caused peak clearly manifests the presence of the notch. Simultaneously, another peak appears in the geometrical center of the measurement zone (Fig. 15(b))

with a greater amplitude than the damage-caused peak, indicating that the external excitation generated by the PZT actuator is also identified [54]. To remove the effect of the external excitation, the region around the excitation is eliminated (Fig. 16(a)). In its planform shown in Fig. 16(b), the location and size of the notch is well characterized: the identified notch is centered at about $\zeta = 0.75$ and $\eta = 0.75$, spanning from about 0.722 to 0.778 in ζ, and from 0.722 to 0.778 in η, respectively, corresponding to the actual region of the notch whose outlines are marked in white.

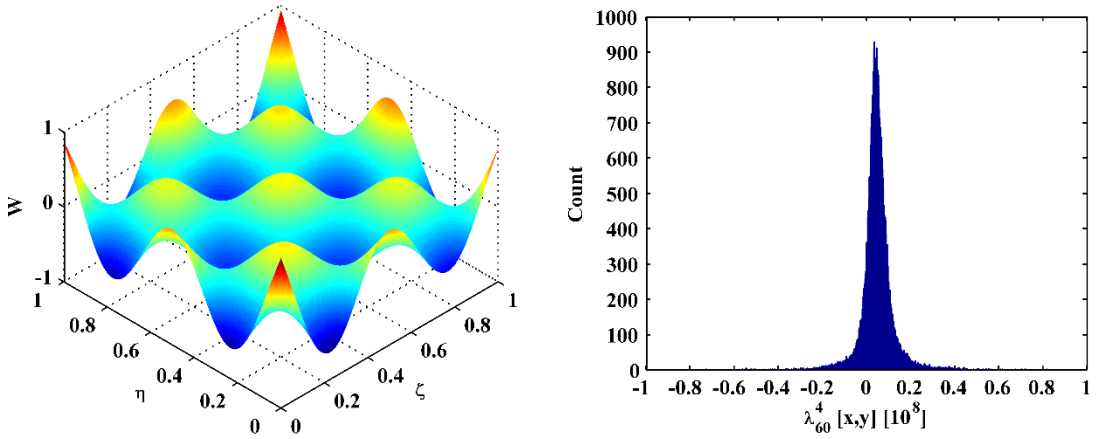

(a) (b)

Fig. 14. (a) Mode shape and (b) statistical distribution of point-wise constant for CFRP laminate with a notch.

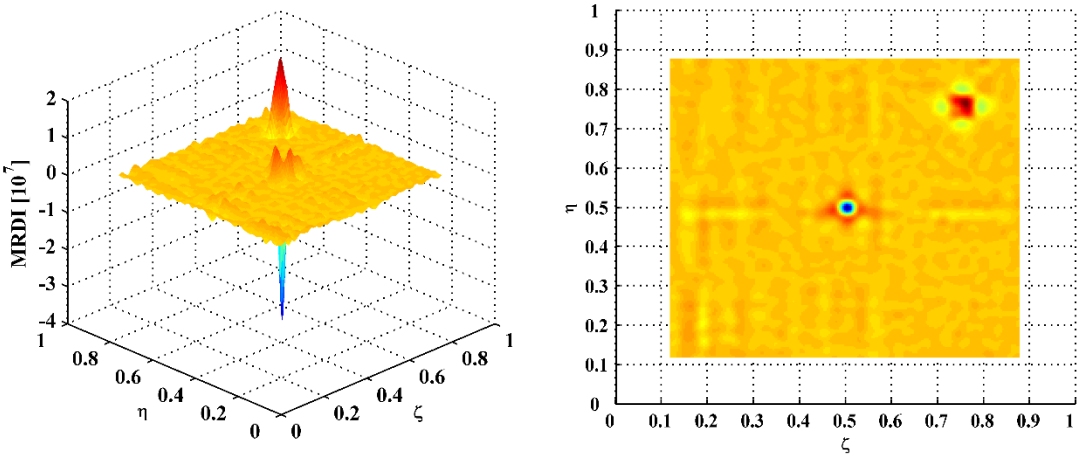

(a) (b)

Fig. 15. (a) Multi-resolution damage index for CFRP laminate with a notch and (b) its planform.

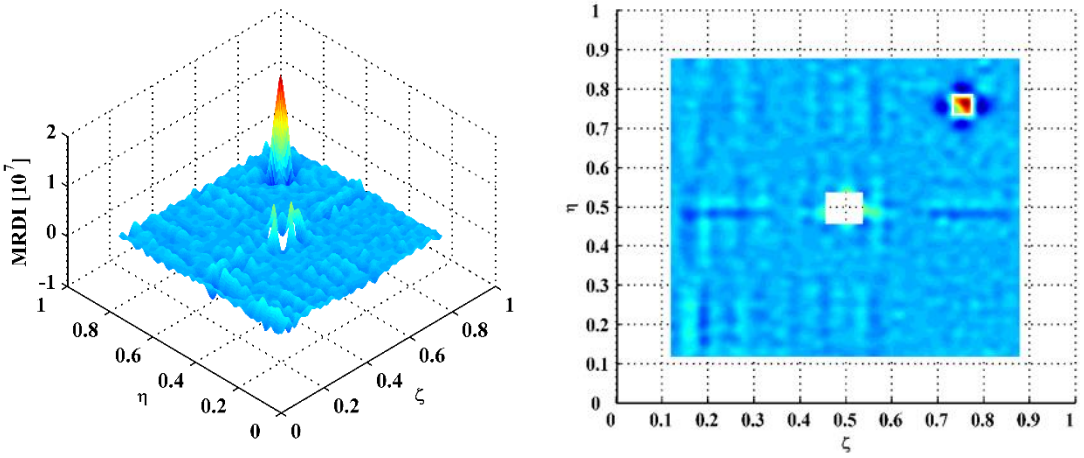

(a) (b)

Fig. 16. (a) Multi-resolution damage index for CFRP laminate with a notch and (b) its planform with excitation region eliminated.

For the CFRP specimen with a delamination, a much higher natural frequency of 3504.7 Hz is selected to produce shorter waves because the delamination is smaller than the notch. It is noteworthy that the sensitivity to damage of a high-order mode depends on the damage location. Therefore, the appropriate natural frequency is selected after several trials to find the corresponding mode that is sensitive to the damage. The ODS is acquired by the SLV subject to harmonic excitation at the natural frequency, which is regarded as the corresponding mode shape and shown in Fig. 17(a) with a unit maximum amplitude. From Eq. (19), the mode shape W is decomposed into its approximation and details at the level of 60 to eliminate the noise components. From Eq. (24), the point-wise constant $\lambda_{60}^4[x,y]$ are calculated and shown in Fig. 17(b); accordingly, the constant λ^4 is determined by $\lambda_{60}^4[x,y]$ being 2.64×10^7 with the maximum count. Then, $MRDI$ is obtained by Eq. (23) and shown in Fig. 18, where a

damage-caused peak clearly indicates the occurrence of the delamination. It is noteworthy that the PZT actuator is placed in the corner of the CFRP laminate. Therefore, the excitation-induced peak in *MRDI* is excluded together with the boundary distortion treatment in the DWT. In the planform of *MRDI* shown in Fig. 18(b), the location and size of the delamination is well characterized: the identified notch is centered at about $\zeta = 0.75$ and $\eta = 0.75$, spanning from about 0.235 to 0.265 in ζ, and from 0.735 to 0.765 in η, in good agreement with the actual location and size of the delamination whose outlines are marked in white.

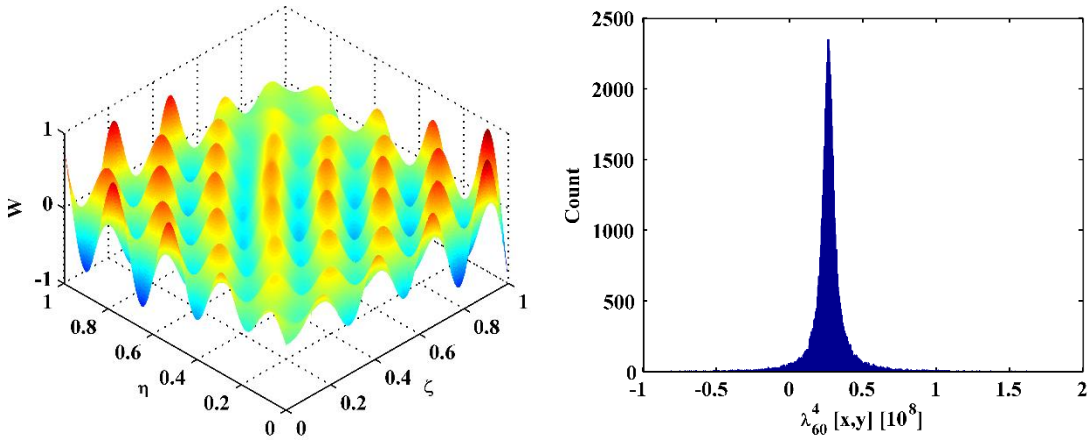

(a) (b)

Fig. 17. (a) Mode shape and (b) statistical distribution of point-wise constant for CFRP laminate with a delamination.

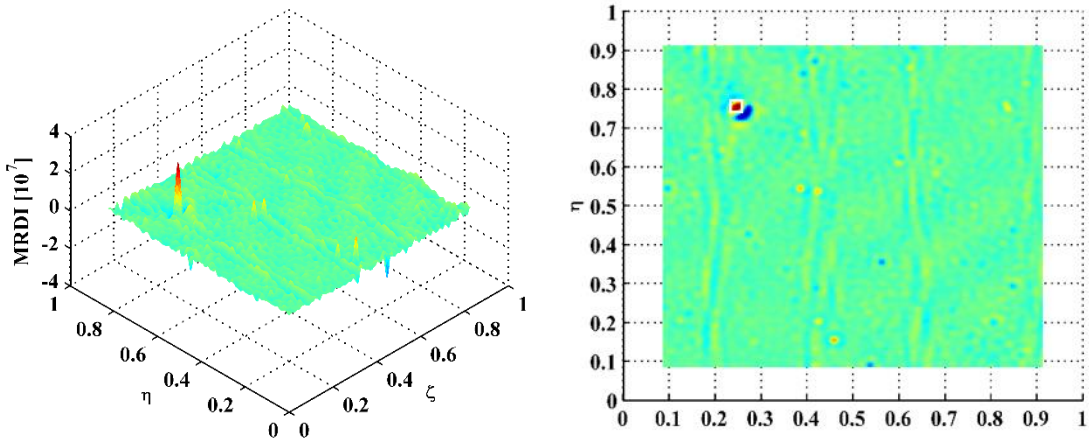

(a) (b)

Fig. 18. (a) Multi-resolution damage index for CFRP laminate with a delamination and (b) its planform.

It is noteworthy that for real-world structural components including composite laminates, damage identification methods relying on laser scanning will encounter some difficulties, such as cost and agility of portage of a SLV for industrial applications and accessibility to structural components that are not easy to inspect. With these concerns, Park et al. [61] discussed the applicability of laser scanning to delamination detection in wind turbine blades. As the SLV has long-range inspection up to 10s of meters, it can be carried on a vehicle to inspect real structural components. For structural components in locations that are not easy to inspect directly, laser beams that scan on the surfaces of inspected components could be reflected from the SLV by mirrors. Thus, applications of the proposed approach to real-world composite components need to be addressed in future study.

5 Concluding remarks

To ensure the integrity and safety of laminated composite structures, it is important to identify initial damage such as notches and delamination before the damage develops. Methods of initial damage identification relying on laser-scanned mode shapes have attracted increasing attention. The pseudo-force/excitation approach has potential for the identification of initial damage in plate-like structures. However, its application in orthotropic and cross-ply composite laminates is limited because it is based on the vibration of isotropic elements. With this concern, a damage characterization approach is developed to fill the gap between the pseudo-force/excitation approach and orthotropic and cross-ply composite laminates in the absence of material and structural

information. In particular, starting from the vibration equation of composite laminates, this study formulates the concept of DF, on which basis a multi-resolution damage index is established for damage identification in composite laminates without knowledge of material and structural parameters. The capability of the approach is numerically verified by the FE method on CFRP laminates with a notch and a delamination, respectively. The applicability of the approach is experimentally validated by identifying a notch and a delamination in CFRP laminates, respectively. The CFRP laminates are excited by PZT actuators and scanned by the SLV to acquire high-resolution mode shapes. Some conclusions are drawn as follows:

(1) Starting from the vibration equation of composite laminates, the concept of DF is formulated, that appears in the damage region and vanishes elsewhere. The DF can be analytically expressed when material and structural parameters are known. In most real-world composite structures, however, these parameters are usually absent. With this concern, strategies of isotropization and normalization are integrated into the vibration equation of composite laminates, to deal with unknown structural and material parameters, respectively. Based on the DF, a parameter-free damage index is established to characterize the presence, location and size of initial damage in composite laminates.

(2) As environmental noise components are inevitably involved in measured mode shapes during measurement and amplified by the differentiating operation when calculating the damage index, actual damage-caused peaks in the DF can be masked by intense noise interference. To remove noise contamination in measured mode shapes, the MRA is integrated into the damage index to form a multi-resolution damage index with higher noise robustness. Noise components can be eliminated while damage features are retained at a satisficing MRA level, making a multi-resolution damage index robust for damage identification in composite laminates in noisy conditions.

(3) The experimental results show that external excitation can be also identified as well as the DF, whose peak in the multi-resolution damage index is more evident with a greater amplitude than the peak of the DF. To remove the effect of the excitation, two strategies are proposed in this study: the first is to eliminate the region around the external excitation in the results; the second is to place the excitation in the corner of the specimen, whereby the excitation-induced peak is excluded, together with the boundary distortion treatment in the DWT.

Acknowledgements

This work is supported by the National Natural Science Foundation of China (Nos. 11772115, 51708173, 51875492, and 51635008) and the China Postdoctoral Science Foundation (No. 2018T110433). Dr. Xu is particularly grateful for the fellowship provided by the Hong Kong Scholars Program (No. XJ2018042).

References:

[1] Z. Zhang, J. Pan, W. Luo, K.R. Ramakrishnan, H.K. Singh, Vibration-based delamination detection in curved composite plates, *Composites Part A: Applied Science and Manufacturing*, 119 (2019) 261-274.

[2] E. Sitnikova, S. Li, D. Li, X. Yi, Subtle features of delamination in cross-ply laminates due to low speed impact, *Composites Science and Technology*, 149 (2017) 149-158.

[3] W.J. Cantwell, J. Morton, Detection of impact damage in CFRP laminates, *Composite Structures*, 3(3-4) (1985) 241-257.

[4] J.P. Komorowski, D.L. Simpson, R.W. Gould, A technique for rapid impact damage detection with implication for composite aircraft structures, *Composites*, 21 (1990) 169-173.

[5] M.V. Hosur, C. Murthy, T.S. Ramamurthy, A. Shet, Estimation of impact-induced damage in CFRP laminates through ultrasonic imaging, *NDT & E International*, 31 (1998) 359-374.

[6] H. Tsutsui, A. Kawamata, J. Kimoto, A. Isoe, Y. Hirose, T. Sanda, N. Takeda, Impact damage detection system using small-diameter optical-fiber sensors embedded in CFRP laminate structures, *Advanced Composite Materials*, 13 (2004) 43-55.

[7] H. Tsutsui, A. Kawamata, T. Sanda, N. Takeda, Detection of impact damage of stiffened composite panels using embedded small-diameter optical fibers, *Smart Materials and Structures*, 13 (2004) 1284-1290.

[8] S. Takeda, S. Minakuchi, Y. Okabe, N. Takeda, Delamination monitoring of

laminated composites subjected to low-velocity impact using small-diameter FBG sensors, *Composites Part A: Applied Science and Manufacturing*, 36 (2005) 903-908.

[9] J. Frieden, J. Cugnoni, J. Botsis, T. Gmuer, Low energy impact damage monitoring of composites using dynamic strain signals from FBG sensors - Part I: Impact detection and localization, *Composite Structures*, 94 (2012) 438-445.

[10] J. Frieden, J. Cugnoni, J. Botsis, T. Gmuer, Low energy impact damage monitoring of composites using dynamic strain signals from FBG sensors - Part II: Damage identification, *Composite Structures*, 94 (2012) 593-600.

[11] D. Graham, P. Maas, G.B. Donaldson, C. Carr, Impact damage detection in carbon fibre composites using HTS SQUIDs and neural networks, *NDT and E International*, 37 (2004) 565-570.

[12] T. Liang, W. Ren, G.Y. Tian, M. Elradi, Y. Gao, Low energy impact damage detection in CFRP using eddy current pulsed thermography, *Composite Structures*, 143 (2016) 352-361.

[13] N. Angelidis, P.E. Irving, Detection of impact damage in CFRP laminates by means of electrical potential techniques, *Composites Science and Technology*, 67 (2007) 594-604.

[14] R.J. Ball, D.P. Almond, The detection and measurement of impact damage in thick carbon fibre reinforced laminates by transient thermography, *NDT & E International*, 31 (1998) 165-173.

[15] T.J. Barden, D.P. Almond, S.G. Pickering, M. Morbidini, P. Cawley, Detection

of impact damage in CFRP composites by thermosonics, *Nondestructive Testing and Evaluation*, 22 (2007) 71-82.

[16] L. Pieczonka, F. Aymerich, G. Brozek, M. Szwedo, W.J. Staszewski, T. Uhl, Modelling and numerical simulations of vibrothermography for impact damage detection in composites structures, *Structural Control and Health Monitoring*, 20 (2013) 626-638.

[17] A. Maier, R. Schmidt, B. Oswald-Tranta, R. Schledjewski, Non-destructive thermography analysis of impact damage on large-scale CFRP automotive parts, *Materials*, 7 (2014) 413-429.

[18] J. Gryzagoridis, D. Findeis, Impact damage detection on composites using optical NDT techniques, *Insight*, 52 (2010) 248-251.

[19] Z. Su, L. Ye, Fundamental lamb mode-based delamination detection for CF/EP composite laminates using distributed piezoelectrics, *Structural Health Monitoring-An International Journal*, 3 (2004) 43-68.

[20] Z. Su, L. Ye, Lamb wave-based quantitative identification of delamination in CF/EP composite structures using artificial neural algorithm, *Composite Structures*, 66 (2004) 627-637.

[21] Z. Su, L. Ye, Y. Lu, Guided Lamb waves for identification of damage in composite structures: A review, *Journal of Sound and Vibration*, 295 (2006) 753-780.

[22] N. Pan, Z. Su, L. Ye, L. Zhou, Y. Lu, A quantitative identification approach for delamination in laminated composite beams using digital damage fingerprints

(DDFs), *Composite Structures*, 75 (2006) 559-570.

[23] Z. Su, C. Yang, N. Pan, L. Ye, L. Zhou, Assessment of delamination in composite beams using shear horizontal (SH) wave mode, *Composites Science and Technology*, 67 (2007) 244-251.

[24] I. Solodov, G. Busse, Nonlinear air-coupled emission: The signature to reveal and image microdamage in solid materials, *Applied Physics Letters*, 91 (2007) 251910.

[25] U. Polimeno, M. Meo, Detecting barely visible impact damage detection on aircraft composites structures, *Composite Structures*, 91 (2009) 398-402.

[26] F. Aymerich, W.J. Staszewski, Impact damage detection in composite laminates using nonlinear acoustics, *Composites Part A: Applied Science and Manufacturing*, 41 (2010) 1084-1092.

[27] A. Klepka, W.J. Staszewski, D. di Maio, F. Scarpa, Impact damage detection in composite chiral sandwich panels using nonlinear vibro-acoustic modulations, *Smart Materials and Structures*, 22 (2013) 084011.

[28] L. Pieczonka, P. Ukowski, A. Klepka, W.J. Staszewski, T. Uhl, F. Aymerich, Impact damage detection in light composite sandwich panels using piezo-based nonlinear vibro-acoustic modulations, *Smart Materials and Structures*, 23 (2014) 105021.

[29] W. Fan, P. Qiao, Vibration-based damage identification methods: A review and comparative study *Structural Health Monitoring-An International Journal*, 10 (2011) 83-111.

[30] P. Qiao, K. Lu, W. Lestari, J. Wang, Curvature mode shape-based damage detection in composite laminated plates, *Composite Structures*, 80 (2007) 409-428.

[31] J.V. Araújo dos Santos, H.M.R. Lopes, M. Vaz, C.M.M. Soares, C.A.M. Soares, M.J.M. De Freitas, Damage localization in laminated composite plates using mode shapes measured by pulsed TV holography, *Composite Structures*, 76 (2006) 272-281.

[32] M.A. Pérez, L. Gil, S. Oller, Impact damage identification in composite laminates using vibration testing, *Composite Structures*, 108 (2014) 267-276.

[33] W. Xu, M. Cao, X. Li, M. Radzieński, W. Ostachowicz, R. Bai, Delamination monitoring in CFRP laminated plates under noisy conditions using complex-wavelet 2D curvature mode shapes, *Smart Material and Structures*, 26 (2017) 104008.

[34] D. Chen, Y. Xu, W. Zhu, Non-model-based identification of delamination in laminated composite plates using a continuously scanning laser Doppler vibrometer system, *Journal of Vibration and Acoustics*, 140(4) (2018) 041001.

[35] Z.B. Yang, M. Radzienski, P. Kudela, W. Ostachowicz, Two-dimensional modal curvature estimation via Fourier spectral method for damage detection, *Composite Structures*, 148 (2016) 155-167.

[36] Z.B. Yang, M. Radzienski, P. Kudela, W. Ostachowicz, Two-dimensional Chebyshev pseudo spectral modal curvature and its application in damage detection for composite plates, *Composite Structures*, 168 (2017) 372-383.

[37] S. Cao, H. Ouyang, L. Cheng, Baseline‐free multidamage identification in plate‐like structures by using multiscale approach and low‐rank modelling, *Structural Control and Health Monitoring*, 26 (2019) e2293.

[38] S. Cao, H. Ouyang, L. Cheng, Baseline-free adaptive damage localization of plate-type structures by using robust PCA and Gaussian smoothing, *Mechanical Systems and Signal Processing*, 122 (2019) 232-246.

[39] D.M. Chen, Y.F. Xu, W.D. Zhu, Experimental investigation of notch-type damage identification with a curvature-based method by using a continuously scanning laser Doppler vibrometer system, *Journal of Nondestructive Evaluation*, 36 (2017) 38.

[40] M. Cao, W. Ostachowicz, M. Radzieński, W. Xu, Multiscale shear-strain gradient for detecting delamination in composite laminates, *Applied Physics Letters*, 103 (2013) 101910.

[41] W. Xu, H. Fang, M. Cao, L. Zhou, Q. Wang, W. Ostachowicz, A noise-robust damage indicator for characterizing singularity of mode shapes for incipient delamination identification in CFRP laminates, *Mechanical Systems and Signal Processing*, 121 (2019) 183-200.

[42] W. Xu, Z. Su, J. Liu, M. Cao, M., W. Ostachowicz, Singular energy component for identification of initial delamination in CFRP laminates through piezoelectric actuation and non-contact measurement, *Smart Materials and Structures*, (2020), in press.

[43] H. Xu, L. Cheng, Z. Su, J-L. Guyader, Identification of structural damage based

on locally perturbed dynamic equilibrium with an application to beam component, *Journal of Sound and Vibration*, 330 (2011) 5963–5981.

[44] M. Cao, L. Cheng, Z. Su, H. Xu, A multi-scale pseudo-force model in wavelet domain for identification of damage in structural components, *Mechanical Systems and Signal Processing*, 28 (2012) 638–659.

[45] M. Cao, Z. Su, L. Cheng, H. Xu, A multi-scale pseudo-force model for characterization of damage in beam components with unknown material and structural parameters, *Journal of Sound and Vibration*, 332 (2013) 5566–5583.

[46] H. Xu, Z. Su, L. Cheng, J-L. Guyader, P. Hamelin, Reconstructing interfacial force distribution for identification of multi-debonding in steel-reinforced concrete structures using noncontact laser vibrometry, *Structural Health Monitoring-An International Journal*, 12(5-6) (2013) 507–521.

[47] H. Xu, Z. Su, L. Cheng, J-L. Guyader, A "Pseudo-excitation" approach for structural damage identification: From "Strong" to "Weak" modality, *Journal of Sound and Vibration*, 337 (2015) 181–198.

[48] H. Xu, Z. Su, L. Cheng, J-L. Guyader, On a hybrid use of structural vibration signatures for damage identification: a virtual vibration deflection (VVD) method, *Journal of Vibration and Control*, 23(4) (2017) 615-631.

[49] H. Xu, B. Lu, Z. Su, L. Cheng, Statistical enhancement of a dynamic equilibrium-based damage identification strategy: Theory and experimental validation, *Journal of Sound and Vibration*, 351 (2015) 236–250.

[50] H. Xu, L. Cheng, Z. Su, J-L. Guyader, Damage visualization based on local

dynamic perturbation: Theory and application to characterization of multi-damage in a plane structure, *Journal of Sound and Vibration*, 332 (2013) 3438–3462.

[51] H. Xu, L. Cheng, Z. Su, Suppressing influence of measurement noise on vibration-based damage detection involving higher-order derivatives, *Advances in Structural Engineering*, 16 (1) (2013) 233-244.

[52] H. Xu, Q. Zhou, M. Cao, Z. Su, Z. Wu, A dynamic equilibrium-based damage identification method free of structural baseline parameters experimental validation in a two-dimensional plane structure, *Journal of Aerospace Engineering*, 31(6) (2018) 04018081.

[53] C. Pezerat, J.L. Guyader, Two inverse methods for localization of external sources exciting a beam, *Acta Acustica* 3 (1995) 1–10.

[54] C. Pezerat, J.L. Guyader, Force analysis technique: Reconstruction of force distribution on plates, *Acta Acustica united with Acustica* 86 (2000) 322–332.

[55] A.W. Leissa, M.S. Qatu, Vibration of continuous systems, *McGraw Hill*, 2011.

[56] Y. Zhao, M. Noori, W. Altabey, R. Ghiasi, Z. Wu, A fatigue damage model for FRP composite laminate systems based on stiffness reduction, *Structural Durability & Health Monitoring*, 13 (2019) 85-103.

[57] S. Mallat, A Wavelet Tour of Signal Processing, *Academic Press*, San Diego, 2008.

[58] H.F. Lam, T. Yin, Application of two-dimensional spatial wavelet transform in the detection of an obstructed crack on a thin plate, *Structural Control and Health*

Monitoring, 19 (2012) 260-277.

[59] H. Xu, Z. Zeng, Z. Wu, L. Zhou, Z. Su, Y. Liao, M. Liu, Broadband dynamic responses of flexible carbon black/poly (vinylidene fluoride) nanocomposites: A sensitivity study, *Composites Science and Technology*, 149 (2017) 246-253.

[60] B.J. Schwarz, M.H. Richardson, Introduction to operating deflection shapes, *CSI Reliability Week*, 10 (1999) 121-126.

[61] B. Park, H. Sohn, P. Malinowski, W. Ostachowicz, Delamination localization in wind turbine blades based on adaptive time-of-flight analysis of noncontact laser ultrasonic signals, *Nondestructive Testing and Evaluation*, 32 (2017) 1-20.